Soft Matter

Accepted Manuscript

ROYAL SOCIETY OF CHEMISTRY

www.rsc.org/softmatter

Controlling the characteristics of lamellar liquid crystals using counterion choice, fluorination and temperature†

Matthew J. Pottage,[a] Tamar L. Greaves, [b] Christopher J. Garvey, [c] Stephen T. Mudie [d] and Rico F. Tabor*[a]

The characteristics of robust and highly ordered fluorinated lamellar phases were explored as a function of temperature, counterion identity and fluorination of the surfactant and co-surfactant. Structural and composition effects were probed using a combination of small-angle scattering of X-rays and neutrons, polarising microscopy and calorimetry. It was found that in general, the phases remained remarkably stable with increasing temperature, showing only moderate loss of order and increased membrane flexibility. By changing the surfactant's cationic counterion, it was possible to exert influence on both the shape of micelles formed and the inter-layer spacing of the lamellar phases obtained. Ordering and crystallinity of the lamellar membranes could be controlled by the level of fluorination of both the surfactant and co-surfactant. These results suggest that subtle manipulations of selected control parameters including co-surfactant selection and counterion choice can provide a high level of control over membrane spacing and local order within lamellar phases, providing guidance where these materials are used as templates.

Introduction

Self-assembled lamellar mesophases have attracted interest in a range of applications, from controlled diffusion and release to lubrication and templating. Their layered characteristics provide an environment in which diffusion can be restricted to a pseudo-2-dimensional state, where molecules can rapidly diffuse within the water or oil spaces inside the sheet-like lamellar membranes, but 'hopping' between layers is unfavoured.[1,2] Additionally, their structural similarity to lipid bilayers makes their use as model systems for biological processes of clear interest. These features, combined with often favourable viscosity and processing properties compared to cubic and other bicontinuous phases have led to a continued research effort in food science[3] and drug delivery.[4]

Fluorination has long been a valuable tool for introducing specific properties to molecules, due to the unique chemistry imparted by the replacement of hydrogen with fluorine.[5,6] In particular, fluorinated amphiphiles have recieved significant attention, both for their own unique properties and due to their role in the syntheses of other fluorinated materials such as fluoropolymers.[6] Due to the strong carbon-fluorine bond and larger volume of the fluorine atom, the properties of fluorinated amphiphiles differ significantly from their hydrocarbon counterparts:[7] they are more hydrophobic and therefore typically have lower solubilities, have a greater surface activity and are also highly stable, both chemically and thermally. However, due to their high stability, their use has become problematic as they are difficult and expensive to synthesise[8] and are potentially highly persistent environmental pollutants.[9]

Due to the bulky and rigid fluorocarbon chain, fluorinated amphiphiles readily adopt low curvature interfaces.[10] However, variations can be observed due to counterion effects. The perfluorooctanoate anion, for example, forms a lamellar phase in water for the lithium[11,12], rubidium,[13] caesium[12,14] and ammonium,[13,15–17] while for the salts of sodium and potassium the lamellar phase isn't observed. Indeed the sodium salt has been found to only form spherical micelles up to the solubility limit.[18,19] While such counterion effects are well-documented in the literature for both hydrocarbon[20] and fluorocarbon surfactants,[21,22] the effect on ternary self-assembled systems is less studied.

Systems that contain both fluorinated and hydrogenated components have been seen to show unusual properties due to the antipathy of fluorocarbons and hydrocarbons. This demixing can be harnessed to drive the formation of structurally specific polymer particles[23] and templated materials with unique morphological characteristics.[24] However, in the context of reducing fluorination from an environmental perspective, the replacement of fluorocarbon-based stabilisers with hydrocarbon analogues has received less interest, despite its obvious cost and ecological advantages.

Our recent study[25] showed that while the sodium salt of perfluorooctanoate forms only an isotropic micellar phase in

† Electronic Supplementary Information (ESI) available: Further details on SANS and SAXS fitting and supplementary data sets. See DOI: 10.1039/b000000x/

*[a]School of Chemistry, Monash University, Clayton 3800, Australia. Fax: +61 3 9905 4597; Tel: +61 3 9905 4558; E-mail: rico.tabor@monash.edu
[b]School of Applied Sciences, RMIT University, Melbourne, VIC 3000, Australia
[c]Bragg Institute, Australian Nuclear Science and Technology Organisation, Lucas Heights, NSW 2234, Australia
[d]Australian Synchrotron, 800 Blackburn Rd, Clayton VIC 3169, Australia

water, the addition of a partially fluorianted co-surfactant, 1H,1H,2H,2H-perfluorooctanol, resulted in a highly ordered lamellar phase. This lamellar mesophase was of interest due to its high zero-shear viscosity and formation at unusually low co-surfactant concentrations. The behaviour was rationalised by the effective charge screening induced by the co-surfactant along with the geometric implications of its intercalation between surfactant molecules.

In this work, we explore the effects of temperature and surfactant counterion identity on phases formed by the pefluorooctanoate anion in water. We investigate a range of counterions from small, hard cations such as lithium to organic species including ammonium and ethylammonium. As an additional control mechanism, we explore the effects of reducing the fluorination within these systems, demonstrating several methods by which structural characteristics can be manipulated.

Materials and methods

Materials: The perfluorooctanoate salts of sodium (NaPFO), lithium (LiPFO), rubidium (RbPFO), ammonium (AmPFO) and ethylammonium perfluorooctanoate[26] (EaPFO) were prepared from perfluorooctanoic acid (99%, Fluorochem, UK) by stoichiometric neutralisation in ultrapure water using standard sodium hydroxide (Merck, 99%), lithium hydroxide (produced from Li metal (>99.9%)), rubidium hydroxide(Sigma, 98%), ammonia (Sigma, 98%) and ethylamine solutions (Sigma, 98%), all used as recieved. The co-surfactant 1H,1H,2H,2H-perfluorooctan-1-ol (PFOH, 99%) was obtained from Fluorochem, and ultrapure water was obtained from a Millipore Direct-Q 5, with a minimal resistivity of 18.2 MΩ·cm. For neutron scattering experiments, D_2O was obtained from Sigma-Aldrich (99.98 atom% D) and used as received.

Small-angle scattering: SAXS experiments were performed on the SAXS/WAXS beamline at the Australian Synchrotron, Clayton, Australia. Samples were prepared in ultrapure H_2O and analysed in capillary sample holders. Temperature was controlled by a recirculating water bath, and monitored *in situ* using a thermocouple sensor placed in the sample holder.

SANS measurements were made on the Quokka beamline at ANSTO, Lucas Heights, Australia. Samples were prepared in 2mm thick cells using D_2O and analysed at a sample temperature of 25°C. In both cases, data were reduced from the raw counts on a two dimensional detector to radially averaged absolute intensity versus the scattering vector q, under the assumption of isotropic scattering, where q is defined:

$$q = \frac{4\pi}{\lambda} \sin \frac{\theta}{2} \quad (1)$$

wherein λ is the wavelength of the incident neutron beam and θ is the scattering angle. Thus the q range is defined by the instrument configurations and the size of the detector. On Quokka, an incident wavelength of λ = 5 Å ($\Delta\lambda/\lambda = 10$) was used with two sample-detector distances of 2 and 14 m, giving a q-range of 0.005-0.400 $Å^{-1}$. To reduce the raw data, the response of each detector pixel was normalised by comparison with the response of the detector to a flat scatterer, and then the scattering from an empty SANS cell was subtracted. The radial average of the intensity expressed as a function of q could then be obtained using the instrument configuration and detector characteristics. The absolute intensity scale was provided by normalising to the sample thickness (2 mm) and comparing the intensity to that of an empty beam measurement. For SAXS, the wavelength of the incident X-rays was 0.62 $Å^{-1}$ with a sample-detector distance 7.34 m, giving a q-range of 0.004-0.273 $Å^{-1}$, and the data reduced as above with the scattered intensity from an empty capillary subtracted as a background.

Data for micelles were modelled using a form factor model for scattering from homogeneous ellipsoids with a Hansen-Hayter-Penfold-Ginoza mean square approximation structure factor for charged spheres interacting *via* a screened Coulomb potential.[27,28] SANS spectra with lamellar characteristics were modelled using the paracrystalline stack model proposed by Nallet, Laversanne and Roux.[29] The application of this model to the study of fluorinated lamellar phases has been covered in detail recently.[25]

Polarising light miscroscopy: Polarising light microscopy (PLM) images were obtained using a CCD camera (Flea3, Point Grey, Richmond, BC, Canada) coupled to a Kozo XJP 300 polarising microscope. Temperature control was achieved using a resistor heated slide mount, with the sample temperature at the time of imaging being recorded using a thermocouple.

Differential Scanning Calorimetry: Differential scanning calorimetry was performed on a DSC Q100 series instrument from TA Instruments using 5mg of sample in a closed aluminium pan. The sample was cooled to 10°C using an attached sample cooling system, then scanned up to 70°C. The scan rate was 10°C/min and the instrument was calibrated using an indium standard.

Results and discussion

We previously showed that although sodium perfluorooctanoate (NaPFO) in water formed only normal micelles until its solubility limit, even very small loadings (< 1wt%) of 1H,1H,2H,2H-perfluorooctan-1-ol (PFOH) resulted in the

formation of lamellar phases.[25] Here we explore the effects of different system parameters on these lamellar phases, using previously delineated compositions as an initial guide to fomulation.

Temperature effects and phase stability

The effects of temperature on PFO/PFOH lamellar phases were explored with two different counter-ions: sodium and ethylammonium, at a range of compositions. The counterions were selected due to having a large contrast in their characteristics, with comparatively small, well-hydrated sodium offering the classical 'hard' cation, whereas the organic and bulky ethylammonium is much more hydrophobic[30]. Typical SAXS spectra are shown in Fig. 1, where panels *a* and *b* show NaPFO and EaPFO phases with high loadings of surfactant and co-surfactant, whereas *c* and *d* represent lower membrane volume fractions (see Table 1 for compositions and fitted parameters from model fitting of SAXS data). EaPFO (also known as EAOF) is an ionic liquid (melting point 58°C), the single-component behaviour of which has been explored previously.[26]

The immediately notable feature is that at high loading, both counter-ions result in phases that are remarkably temperature stable. There were no observed phase changes for either sample over the temperature range measured, and any changes in interlamellar spacing and membrane thickness were sufficiently small as to be neglected. The only structural change was a moderate increase in the Caillé parameter, η_{cp} (Table 1). This parameter is defined in terms of the position of the first Bragg peak q_0, thermal energy k_BT, the membrane bending elastic modulus K and the membrane compression modulus $\bar{B}$:

$$\eta_{cp} = \frac{q_0^2 k_B T}{8\pi\sqrt{K\bar{B}}} \qquad (2)$$

If we consider that the bulk compression modulus for a condensed phase is unlikely to change significantly for a fixed composition, then an *increase* in Caillé parameter would reflect a *decrease* in membrane bending elastic modulus – that is, more flexible lamellar membranes. This could certainly be expected with increasing temperature due to reduced 'crystallinity' or chain packing order within the highly structured fluorocarbon membranes. It is notable that there is a general lack of fit at low q to the Nallet model[29] for the phases explored here. This region reflects scattering from large length-scales, usually interpreted in the Nallet model as resulting from correlations within the membrane.[31–34]

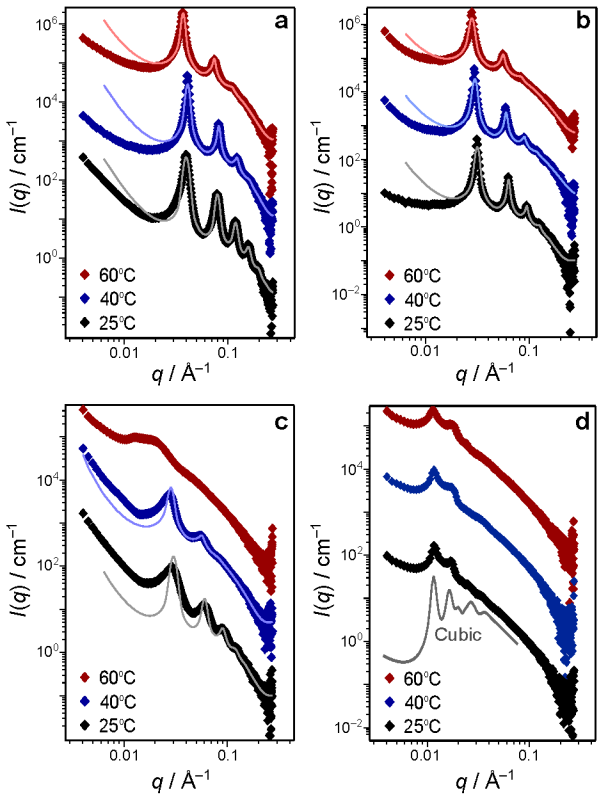

Fig. 1 SAXS analysis of NaPFO (M19, M16) and EaPFO (E19, E16) lamellar mesophases with PFOH at high surfactant/co-surfactant concentration (a) and (b), and low concentration (c) and (d) as a function of temperature. Data sets are offset vertically for clarity of presentation. Compositions and obtained parameters from model fits to data (where shown) are given in Table 1. A model prediction for a primitive cubic phase with apparently similar dimensions to the scattering seen in (d) is provided for comparison.

At lower loadings of surfactant and co-surfactant (Fig. 1c,d), significantly less ordered phases are produced, and it is clear that the Nallet model[29] is not entirely able to capture the characteristics of these weakly ordered phases. With a sodium counterion (Fig. 1c), the apparent rigidity of the lamellar membranes is reduced, as evidenced by the higher Caillé parameter. The quality of fit for these spectra at low q is comparatively low, and so although the interlamellar spacing remains accurately defined by the position of the first Bragg peak, the Caillé parameter should be assumed to have an uncertainty of at least 10%. It also appears that the overall order of the lamellar phase is lower, as evidenced by the more rapid decrease in peak intensity for higher order peaks at larger q. In this case, an increase in temperature to 60°C results in an apparent phase change. The resulting phase appears to share a characteristic q^{-4} slope at low q,

Table 1 Compositional and fitted parameters for selected phases shown in Fig. 1: sample name (Spl), mass fractions of water (H_2O), surfactant (Surf.) and co-surfactant (PFOH), interlamellar spacing (d), Caillé parameter (η_{cp}) and membrane thickness (δ). For samples M16 and M19, the surfactant was NaPFO; for samples E16 and E19, it was EaPFO.

Spl	H_2O	Surf.	PFOH	T/°C	d/Å	η_{cp}	δ/Å
M19	0.83	0.07	0.10	25	158	0.05	22
				40	153	0.12	22
				60	169	0.20	22
E19	0.83	0.07	0.10	25	200	0.10	25
				40	211	0.13	20
				60	225	0.20	22
M16	0.93	0.035	0.035	25	208	0.10	24
				40	220	0.30	25
				60	-	-	-
E16	0.93	0.035	0.035	25	-	-	-
				40	-	-	-
				60	-	-	-

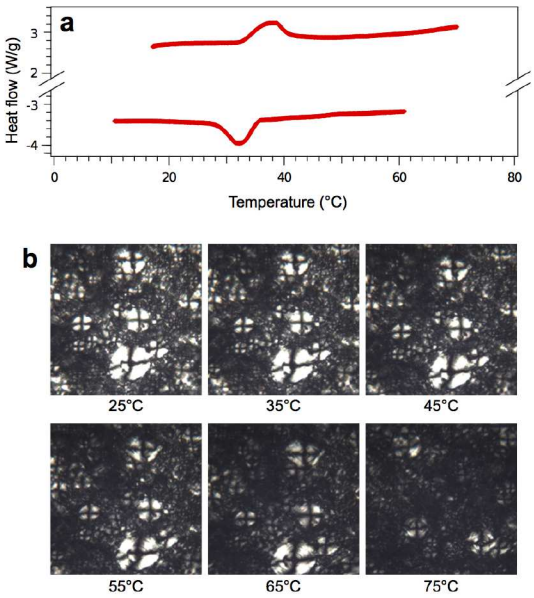

Fig. 2 Thermal response of fluorinated lamellar phases. a) DSC data for sample M19 (composition defined in Table 1). b) Temperature-dependent polarising light micrographs of M19 between crossed polarisers.

characteristic of extended surfaces, but also contains multiple poorly-defined features that may represent coexistence of several kinetically trapped phases, as seen previously for these materials.[25]

In contrast, the phase produced with the same concentration of EaOF and PFOH (Fig. 1d) shows distinctly different characteristics, and does not fit to a simple lamellar 'stack' model. Without well-resolved higher q peaks to provide additional information, it is difficult to unequivocally assign the phase present in Fig. 1d, as it could be a mixture of two lamellar phases with different spacings,[35–37] or a cubic phase. The fact that the scattering pattern is comparatively invariant with temperature suggests that the peaks do not represent a phase coexistence, but rather that the sample contains a single, isotropic phase. This was corroborated by the visual appearance of the sample; microscopy between crossed polarisers did not reveal any significant birefringence. Thus the most likely candidate is the non-birefringent cubic phase. The predicted scattering from a simple cubic arrangement of spheres[38,39] that assumes the primary peak represents the inter-sphere spacing is shown as a solid line in Fig. 1 for comparison.

In order to explore the rationale for a decreased bending modulus with increasing temperature, we measured the thermal response of a typical phase using differential scanning calorimetry (DSC) and polarising light microscopy (PLM) with results shown in Fig. 2. The results of DSC studies were fairly consistent between compositions, showing no sharp peaks in the 0-80°C range that would indicate phase transitions. However, in each case, a small peak was noted between 30 and 40 degrees, with an example for sample M19 shown in Fig. 2a. Following the temperature-dependent behaviour of the same sample with polarising light microscopy (Fig. 2b) corroborates the lack of phase transitions in this region. Note that the characteristic 'Maltese cross' are somewhat distorted, possibly due to the effects of compressing the highly viscous sample between a slide and cover slip.

It is likely that the small (but reproducible) feature seen in the DSC traces of these systems represents a 'chain melting' effect in the perfluorocarbon membranes, where the layers transition from a somewhat crystalline to more fluid state. This phenomenon has been noted in similar fluorosurfactants previously by Hoffman and Würtz.[40] Such effects are well-understood and investigated for lipid bilayer systems, where the effects of melting point of the constituent lipids control the membrane fluidity.[41] This would also explain the broadening of peaks and general loss of order seen in Fig. 1 and the slow decrease in overall birefringence seen in Fig. 2b.

Effects of changing surfactant counterion

The effects of varying counterion on surfactant phase behaviour and the structural characteristics of self-assembled

mesophases are well-document for many molecules.[37,42] The wealth of literature provides ample guidance for the interpretation of such relationships for other systems. For example, a recent elegant investigation of counterion effects for surfactants with cationic ammonium headgroups found decreased interfacial curvature when moving from small inorganic to larger, organic counterions.[43] Previous investigations of various perfluorooctanoate species indicate a significant effect of counterion selection on surfactant properties (Table 2).

Table 2 Selected physicochemical parameters of the perfluorooctanoate anion with different counterions: Krafft temperature T_{Kr}, critical micelle concentration CMC, and cation hydrated ionic radius r_{hyd}.

Surf.	$T_{Kr}/^{\circ}$C	CMC / mol L^{-1}	r_{hyd} /pm
LiPFO	$<0^a$	0.0311^c	382^d
NaPFO	8.0^a	0.036^a	358^d
RbPFO	20.2^a	0.028^a	329^d
AmPFO	2.5^a	0.033^a	331^d
EaPFO	$<0^b$	-	417^b
HPFO	20^a	0.009^a	-

[a]from Nakayama.[44] [b]measured or calculated in this work. [c]from Bernazzani *et al.*[45] [d]from Conway.[46]

Of particlar interest is the characteristic trend in Krafft point with hydrated ion radius, whereby large, diffuse or well-hydrated ions (*e.g.* lithium, ethylammonim) are soluble at much lower temperatures than the smaller, poorly-hydrated counterparts (*e.g.* rubidium). Conversely, the CMC is rather unaffected by cation choice, rationalised by the primary drive arising from the hydrophobicity of the fluorinated chains. Headgroup, as expected, has only a minor role to play in this case. The exception is the free acid, HPFO, which has a much lower CMC due to the poor solubility conferred by the weakly dissociating proton.

Exploring the effects of these different counterions on the shape and structural characteristics of self-assembled surfactant phases provides further insight. For simple ions that can be approximated as spheres, different properties arise due to difference in size and charge density, while for bulkier ions such as quartenary ammonium compounds, shape and steric interactions are also a factor.[43] Here we studied the five cations listed in Table 2: lithium, sodium, rubidium, ammonium and ethylammonium. Of these, ethylammonium can be considered to have an anisotropic geometry and charge density distribution, whereas the remainder are spherical ions.

For aqueous surfactant solutions, (*i.e.* binary surfactant-water systems with no co-surfactant added), the change in counterion was found to have a profound effect on the geometry of the PFO aggregates at 5 wt% loading (Fig. 3a), and therefore also the aggregation number. Aggregation numbers, N_{agg}, were calculated by dividing the total micelle volume by the volume occupied by a single surfactant tail-group, after Berr and Jones.[47] For the ethylammonium salt, the scattering profile was best fit using a lamellar model, however it can also be fit well with a highly eccentric ellipsoidal model (essentially approximating a bilayer 'disc'). This simply indicates extended surfaces, *i.e.* a very high aspect ratio. This tendency toward zero curvature interfaces likely results from a combination of electrostatic and geometric effects. As for other ionic surfactant micelles,[48] and other PFO salts (see below) full dissociation is not expected (*i.e.* a proportion of surfactant monomers within each micelle retain their bound counterion. In the case of EaPFO, this bulky counterion may more effective screen the charge repulsion between ionised monomers, thus reducing inter-head-group repulsions and favouring lower curvatures. Equally, the hydrophobic character of the ethyl chain on the counterion could be expected to increase its intercalation further into the bilayer structure when compared to hydrophilic, inorganic ions, meaning that ethylammonium can more effectively penetrate between surfactant molecules, further aiding inter-head-group charge screening and modifying interfacial curvature. The net result of this decreased head-group repulsion is the shift from the high curvature spherical micellar phase through to a low curvature bilayer structure. This can be seen as an effective decrease in head-group area, thus packing parameter considerations also favour the transition to lower curvature interfaces.[49]

The changes in micelle shape and aggregation number seen for the inorganic counterions and ammonia were less extreme than for ethylammonium. However, differences were measurable and relationships are depicted in Fig. 4. There is a clear trend toward more oblate geometries with increasing hydrated ion size, the extreme case of which is the bilayer-type geometry seen for EaOF. This can be partially explained by the intercalation effect described above, although the relationship may not be solely based upon geometry (*i.e.* that larger ions cause a decrease in overall curvature, favouring oblate or bilayer geometries). An additional factor is the level of dissociation, as ionic surfactant monomers are known to be only partially dissociated when aggregated in micelles.[43] Calculated levels of dissociation, α, from modelling of SANS/SAXS data are given in Table 3, where α = number of dissociated surfactant monomers in micelle / total number of surfactant monomers in micelle. The greater the level of dissociation, the smaller micelles tend to be, as high charge densities tend to favour higher curvature intefaces. Thus there

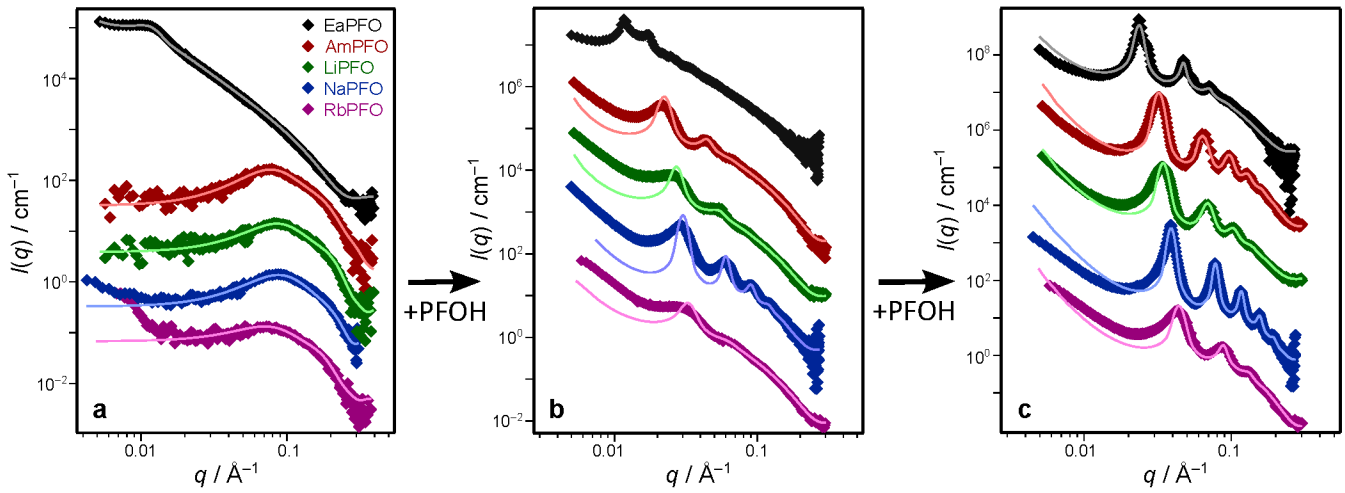

Fig. 3 SANS and SAXS spectra of PFO/PFOH phases: a) 5% perfluorooctanoate solutions with varying counterions and the phases formed upon the addition of the fluoroalcohol PFOH at b) low volume fraction of surfactant and alcohol (volume fraction, $\Phi = 0.038$) and c) higher volume fraction ($\Phi = 0.100$.) In all cases, symbols represent the experimental SANS/SAXS data points, and solid lines are fits to the data as described in the text. All measurements were made at 25°C and profiles are vertically offset by multiplication for clarity of presentation.

is a clear correlation between aggregation number and level of dissociation (Fig. 4b).

The increase in intensity at low q for rubidium micelles may represent critical scattering from the formation of larger scale fractal-like aggregates of micelles.[50] This would arise from the low solublity of RbPFO, as evidenced by its high Krafft point (Table 2), with the strong interactions indicating that the system is close to a phase boundary (which in this case would be a normal micellar solution *vs* solid/solution separation).

When combined with the co-surfactant PFOH, all species formed stable, isotropic phases, with superficially similar characteristics. Only when observing the scattering profiles (Fig. 3b,c) were the structural differences apparent. As in the temperature analysis, two compositions were analysed: a low ($\Phi = 0.038$) and high ($\Phi = 0.100$) volume fraction, where precise compositions and fitting parameters are outlined in Table 3. For both compositions, the change in counterion led to a change in the interlamellar spacing, which observed the same trend at both low and high volume fraction. As expected from previous studies of these systems,[25] the lamellar phases formed were significantly more ordered and more rigid at higher volume fractions, as evidenced by the relative peak intensities with increasing q and the low Caillé parameters (Table 3).

As with the effects on micellar geometry, the counterion characteristics potentially change the lamellar phases in a number of ways. In general, it would be expected that more highly charged membranes – that is, those which posess a greater degree of counterion dissociation – would repel each other more effectively through charge-based interactions, thus increasing lamellar spacing.[37,42] However, the penetration of counterions into the layer itself, which may be more effective for ammonium and ethylammonium variants, may also play a role. In addition, the Caillé parameter is linked to membrane flexibility, which may also be affected by counterion dissociation/penetration and the general packing effectiveness of the surfactant and co-surfactant. The lamellar spacing is plotted as a function of Krafft temperature, which to some degree encompasses the surfactant solubility and therefore ability for counterion dissocation, in Fig. 4c, demonstrating reasonable correlation. Interestingly, the lowest Caillé parameters, indicating the most rigid bilayers, were seen for sodium and ammonium counterions, both of which have intermediate Krafft temperatures of 8 and 2.5°C respectively. This may indicate a favourable 'middle ground' for membrane crystallinity.

Once again, the exception to the observed trends was the ethylammonium ion, which formed a non-lamellar phase (which may be cubic, see above) at low loadings of co-surfactant and a slightly deformed lamellar phase with very large interlamellar spacing at higher loadings. In this case, steric and membrane penetration effects are likely to be more important, indicating that adding organic character to the surfactant counterion provides an additional control parameter for modifying the properties of lamellar liquid crystals.

Table 3 Compositional and fitted model parameters from SANS/SAXS analysis of perfluorooctanoate phases: sample name, mass fractions of water (H_2O), surfactant (Surf.) and co-surfactant (PFOH), interlamellar spacing (d), Caillé parameter (η_{cp}), membrane thickness (δ), micelle principle radii (R_a, R_b), micelle aggregation number (N_{agg}), degree of counterion dissociation (α) and micelle aspect ratio (R_a/R_b).

Sample	H_2O	Surf.	PFOH	d/Å	η_{cp}	δ/Å	R_a, R_b/Å	N_{agg}	α	R_a/R_b
RbPFO	0.95	0.05	-	-	-	-	26, 12	46	0.22	2.20
NaPFO	0.95	0.05	-	-	-	-	14, 15	34	0.63	0.93
LiPFO	0.95	0.05	-	-	-	-	8, 17	28	0.74	0.47
AmPFO	0.95	0.05	-	-	-	-	25, 11	37	0.65	2.30
EaPFO	0.95	0.05	-	522	1.26	21	-	-	-	-
RbPFO	0.93	0.035	0.035	190	0.55	21	-	-	-	-
NaPFO	0.93	0.035	0.035	208	0.10	24	-	-	-	-
LiPFO	0.93	0.035	0.035	230	0.40	22	-	-	-	-
AmPFO	0.93	0.035	0.035	280	0.27	21	-	-	-	-
EaPFO	0.93	0.035	0.035	-	-	-	-	-	-	-
RbPFO	0.80	0.07	0.13	142	0.18	21	-	-	-	-
NaPFO	0.80	0.07	0.13	161	0.05	23	-	-	-	-
LiPFO	0.80	0.07	0.13	182	0.11	23	-	-	-	-
AmPFO	0.80	0.07	0.13	195	0.06	22	-	-	-	-
EaPFO	0.80	0.07	0.13	265	0.16	25	-	-	-	-

Level of fluorination

There is a great deal of valuable information in the literature concerning the antipathy of fluorinated and hydrogenated materials. In particular, this phenomenon has been explored in the context of microemulsion polymerisations,[23] liquid crystals[51] and demixed micelle systems.[52] Here, we explore the effects of replacing the fluorinated surfactant and/or co-surfactant alcohol with their hydrogenated counterparts, sodium octanoate and octan-1-ol, as a (somewhat crude) additional method for controlling the structural characteristics of lamellar phases. An additional motivation is the eventual replacement of fluorinated amphiphiles, due to their environmentally persistent and toxic nature.[9,53] Scattering spectra from the phases formed by a matrix of hydrogenated/fluorinated surfactant and co-surfactant at the same composition (7 wt% surfactant and 10 wt% co-surfactant) are shown in Fig. 5.

It is immediately clear from Fig. 5 that the system comprising fluorinated surfactant and fluorinated alcohol is the most ordered, showing the greatest intensity of higher order peaks and the lowest Caillé value. By replacing the fluorinated alcohol with (hydrogenated) octan-1-ol, the level of order decreases significantly, as does the layer rigidity. This is readily rationalised as an increased membrane fluidity imparted by the much more flexible hydrocarbon chains. Interestingly, there is no evidence of phase separation, indicating that the alcohol is well-mixed with the fluorinated surfactant.

The inverse case, whereby the fluorinated alcohol is mixed with sodium octanoate however, does not produce a stable phase. This may be connected with the significantly higher water solubility of sodium octanoate, as evidenced by its CMC at 300 mM when compared to sodium perfluorooctanoate at 30-36 mM.[25] This indicates that the hydrogenated analogue is less hydrophobic, explaining its inability to stabilise the high loading of highly hydrophobic, fluorinated alcohol. The final case for comparison is the fully hydrogenated system of sodium octanoate and octan-1-ol, which has been studied previously.[54,55] The characteristics of this phase are very similar to the EaPFO/water binary system (Fig. 3a), implying either a very weakly structured lamellar phase or a somewhat oriented system of high aspect ratio bilayer discs. The composition studied here was assigned as lamellar in previous work,[55] although the phase is sufficiently weakly ordered that our data demands a model fit with an excessive Caillé parameter (>1 is considered unphysical based on the assumptions of the model[29]).

It is therefore clear that level of fluorination has an important role in membrane flexibility and fluidity, providing a mechanism for controlling membrane fluidity *without* resulting in a phase change. Concomitant with the increased membrane flexibility however is an increase in interlamellar spacing, reflecting more disordered, less closely packed and less crystalline bilayers.

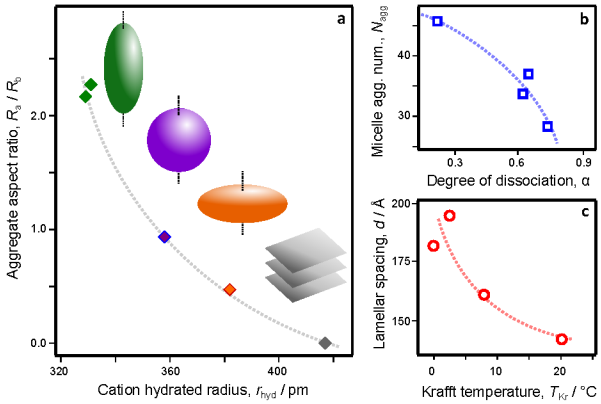

Fig. 4 Counterion effects on fluorosurfactant self assembly. a) Change in aggregate aspect ratio as a function of cation hydrated radius. The inset shapes show the approximate geometries corresponding to each point, where the vertical dotted lines indicate the axis of rotation for the spheroidal geometries. b) Change in micelle aggregation number as a function of the degree of surfactant dissociation within the micelle. c) Change in interlamellar spacing with Krafft temperature. In all cases, dotted lines are drawn as a guide to the eye.

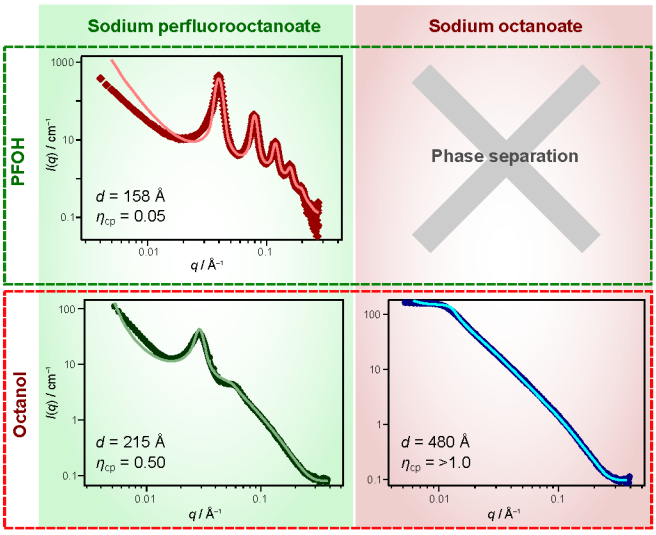

Fig. 5 The effects of level of fluorination on phase characteristics: samples formed by 7 wt% sodium octanoate or perfluorooctanoate and 10 wt% octan-1-ol or 1H,1H,2H,2H-perfluorooctan-1-ol (PFOH). Symbols represent the experimental SANS/SAXS data points, and solid lines are fits to the data as described in the text.

Conclusion

The effects of changing temperature, surfactant counterion and chain chemistry were explored for a fluorinated lamellar phase comprising a variety of perfluorooctanoate surfactants and a partially fluorinated alcohol. Characterisation was made mainly by small-angle X-ray and neutron scattering, providing insight into nanostructural parameters such as inter-membrane spacing, but also the rigidity and order of the membranes.

The fluorinated liquid crystals showed remarkable temperature stability, particularly at higher volume fractions. A small endotherm that was not associated with a phase change was noted at *ca* 35°C, and apportioned to a 'chain melting' transition,[41] reflecting decreased crystallinity of the fluorinated bilayers.

Changing the surfactant counterion was found to have a profound effect on both micelle geometry for the pure surfactants, and layer spacing for lamellar mesophases, in line with expectation from other surfactant studies.[37,42,43] In particular, the ability of a larger organic counterion to interpenetrate the surfactant headgroups,[43] increasing charge screening and therefore decreasing interfacial curvature, was notable. A general correlation between Krafft temperature and inter-membrane spacing indicates that more soluble surfactants tend to favour larger spacings, again rationalised as an effect of increased counterion dissocation leading to more highly charged membranes.

The highly crystalline nature of the fluorinated membranes was highlighted by replacement of the fluorinated surfactant and/or co-surfactant by their hydrogenated counterparts. The fluorinated surfactant was able to stabilise phases with hydrogenated octanol, but the membrane fluidity was significantly increased, as was inter-layer spacing, rationalised as generally less ordered membrane.

These measurements provide insight into the ways in which the spacing and flexibility/fluidity of lamellar membranes can be controlled by subtle manipulations of the surfactant counterion and chain chemistry. Such control parameters are central to the formulation of phases with designed structural characteristics for templating, controlled release and delivery.[4,25]

Acknowledgement

We acknowledge the support of the Bragg Institute, Australian Nuclear Science and Technology Organisation, in providing the neutron research facilities used in this work. Some of this research was undertaken on the SAXS/WAXS beamline at the Australian Synchrotron, Victoria, Australia.

References

1 P. G. Saffman and M. Delbruck, *Proc. Nat. Acad. Sci. U.S.A*, 1975, **72**, 3111–3113.

2 P. Moreau, D. van Effenterre, L. Navailles, F. Nallet and D. Roux, *Eur. Phys. J. E*, 2008, **26**, 225–234.

3 O. R. Fennema, *Food Chemistry*, CRC Press, New York, 3rd edn., 1996.

4 C. M. Chang and R. Bodmeier, in *Bicontinuous Liquid Crystals*, ed. M. L. Lynch and P. T. Spicer, CRC Press, 2005, pp. 321–352.

5 D. M. Lemal, *J. Org. Chem.*, 2004, **69**, 1–11.

6 R. C. Buck, P. M. Murphy and M. Pabon, in *Polyfluorinated Chemicals and Transformation Products*, ed. T. P. Knepper and F. T. Lange, Springer, New York, 2012, ch. Chemistry, Properties, and Uses of Commercial Fluorinated Surfactants.

7 R. F. Tabor, C. Wu, F. Grieser, R. R. Dagastine and D. Y. C. Chan, *J. Phys. Chem. Lett*, 2013, **4**, 3872–3877.

8 R. Fowler, W. Buford III, J. Hamilton Jr., R. Sweet, C. Weber, J. Kasper and I. Litant, *Ind. Eng. Chem.*, 1947, **39**, 292–298.

9 M. M. MacDonald, M. J. A. Dinglasan-Panlilio, S. A. Mabury, K. R. Solomon and P. K. Sibley, *Env. Sci. Tech.*, 2007, **41**, 7159–7163.

10 J. Ravey and M. Stébé, *Colloids Surf. A*, 1994, **84**, 11 – 31.

11 P. Kekicheff and G. J. T. Tiddy, *J. Phys. Chem.*, 1989, **93**, 2520–2526.

12 M. Monduzzi, *Curr. Opin. Colloid Interface Sci.*, 1998, **3**, 467–477.

13 K. Reizlein and H. Hoffmann, *Prog. Colloid Polym. Sci.*, 1984, **69**, 83–93.

14 N. Boden, K. W. Jolley and M. H. Smith, *J. Phys. Chem.*, 1993, **97**, 7678–7690.

15 N. Boden, J. Clements, K. W. Jolley, D. Parker and M. H. Smith, *J. Phys. Chem.*, 1990, **93**, 9096–9105.

16 S. Ristori, G. Gebelb and G. Martini, *Coll. Surf. A*, 1993, **80**, 113–120.

17 G. J. T. Tiddy, *J. Chem. Soc., Faraday Trans. 1*, 1972, **68**, 608–612.

18 Z.-J. Yu and D. Neuman, *Langmuir*, 1994, **10**, 377–380.

19 E. Caponetti, D. Chillura Martino, M. A. Floriano and R. Triolo, *Langmuir*, 1993, **9**, 1193–1200.

20 A. Underwood and E. Anacker, *J. Colloid Interface Sci.*, 1987, **117**, 242 – 250.

21 K. Fontell and B. Lindman, *J. Phys. Chem.*, 1983, **87**, 3289–3297.

22 K. Shinoda, M. Hato and T. Hayashi, *J. Phys. Chem.*, 1972, **76**, 909–914.

23 S. E. Rogers, J. Eastoe, L. Hudson, S. Gold, R. K. Heenan and I. Grillo, *J. Colloid Interface Sci.*, 2009, **330**, 437–442.

24 R. Xing, H. J. Lehmler, B. L. Knutson and S. E. Rankin, *Langmuir*, 2009, **25**, 6489–6492.

25 M. J. Pottage, T. Kusuma, I. Grillo, C. J. Garvey, A. D. Stickland and R. F. Tabor, *Soft Matter*, 2014, **10**, 4902–4912.

26 Y. Shen, D. Kennedy, T. L. Greaves, A. Weerawardena, R. J. Mulder, N. Kirby, G. Song and C. J. Drummond, *Phys. Chem. Chem. Phys.*, 2012, **14**, 7981–7992.

27 C. Wu, D. Y. Chan and R. F. Tabor, *J. Colloid Interface Sci.*, 2014, **426**, 80–82.

28 J. B. Hayter and J. Penfold, *Mol. Phys.*, 1981, **42**, 109–118.

29 F. Nallet, R. Laversanne and D. Roux, *J. Phys. II France*, 1993, **3**, 487–502, available at https://hal.inria.fr/file/index/docid/247849/filename/ajp–jp2v3p487.pdf.

30 P. Niga, D. Wakeham, A. Nelson, G. G. Warr, M. Rutland and R. Atkin, *Langmuir*, 2010, **26**, 8282–8288.

31 *Neutron, X-rays and Light. Scattering Methods Applied to Soft Condensed Matter*, ed. T. Zemb and P. Lindner, North–Holland, Amsterdam, 2002.

32 F. Nettesheim, C. B. Muller, U. Olsson and W. Richtering, *Coll. Poly. Sci.*, 2004, **282**, 918–926.

33 R. F. Tabor, M. I. Zaveer, R. R. Dagastine, I. Grillo and C. J. Garvey, *Langmuir*, 2013, **29**, 3575–3582.

34 F. Castro-Roman, L. Porcar, G. Porte and C. Ligoure, *Eur. Phys. J. E*, 2005, **18**, 259–272.

35 M. Dubois and T. Zemb, *Langmuir*, 1991, **7**, 1352–1360.

36 F. Caboi and M. Monduzzi, *Langmuir*, 1996, **12**, 3548–3556.

37 G. Brotons, M. Dubois, L. Belloni, I. Grillo, T. Narayanan and T. Zemb, *J. Chem. Phys.*, 2005, **123**, 024704.

38 H. Matsuoka, H. Tanaka, T. Hashimoto and I. Norio, *Phys. Rev. B*, 1987, **36**, 1754–1765.

39 H. Matsuoka, H. Tanaka, N. Iizuka, T. Hashimoto and N. Ise, *Phys. Rev. B*, 1990, **41**, 3854–3856.

40 H. Hoffmann and J. Wurtz, *J. Molec. Liquids*, 1997, **72**, 191 – 230.

41 R. B. Gennis, *Biomembranes: Molecular Structure and Function*, Springer, 1989.

42 H. N. Patrick and G. G. Warr, *J. Phys. Chem.*, 1996, **100**, 16268–16274.

43 C. K. Liu and G. G. Warr, *Langmuir*, 2014, DOI:10.1021/la502930p.

44 H. Nakayama, *Bull. Chem. Soc. Jpn.*, 1967, **40**, 1592–1595.

45 L. Bernazzani, R. Carosi, P. Gianni and V. Mollica, *J. Solution Chem.*, 2009, **38**, 1369–1379.

46 B. E. Conway, *Ionic Hydration in Chemistry and Bio-*

physics, Elsevier, 1981.

47 S. S. Berr and R. R. M. Jones, *J. Phys. Chem.*, 1989, **93**, 2555–2558.

48 *Dynamics of Surfactant Self-Assemblies: Micelles, Microemulsions, Vesicles and Lyotropic Phases*, ed. R. Zana, CRC Press, Boca Raton, 2005.

49 J. N. Israelachvili, D. J. Mitchell and B. W. Ninham, *J. Chem. Soc., Faraday Trans. 2*, 1976, **72**, 1525–1568.

50 C. T. Lee, K. A. Smith and T. A. Hatton, *Langmuir*, 2009, **25**, 13784–13794.

51 M. Kadi, P. Hansson, M. Almgren and I. Furó, *Langmuir*, 2002, **18**, 9243–9249.

52 M. Almgren and V. M. Garamus, *J. Phys. Chem. B*, 2005, **109**, 11348–11353.

53 M. Houde, J. W. Martin, R. J. Letcher, K. R. Solomon and D. C. G. Muir, *Env. Sci. Tech.*, 2006, **40**, 3463–3473.

54 P. Ekwall, L. Mandell and K. Fontell, *J. Colloid Interface Sci.*, 1969, **29**, 542–551.

55 D. W. Osborne, *Colloids Surf.*, 1987, **30**, 13–23.

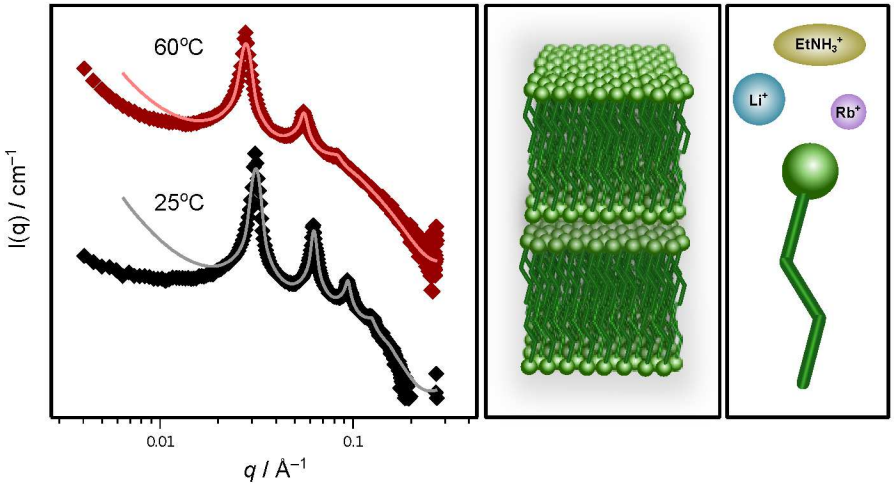

Fig. 6 GRAPHICAL ABSTRACT: The effects of temperature, surfactant counterion, and chain fluorination on lamellar phases are explored, revealing a complex interplay of interactions.